Tight-binding simulations of Nb surfaces and surface defects

Ch. E. Lekka,[1] M. J. Mehl,[2] N. Bernstein,[2] and D. A. Papaconstantopoulos[1,2]
[1]*School of Computational Sciences, George Mason University, Fairfax, Virginia, USA*
[2]*Center for Computational Material Science, Naval Research Laboratory, Washington DC, USA*
(Received 13 March 2003; published 23 July 2003)

We study the properties of low-index Nb surfaces using the NRL-tightbinding (TB) method. We develop a new TB Hamiltonian for Nb using the basic NRL-TB framework with an expanded fitting database that includes additional bulk structures and frozen phonon calculations. The resulting Hamiltonian is validated by comparing to several bulk-zero-temperature and finite temperature properties. Using this Hamiltonian we simulate the three low-index surfaces, (001), (110), and (111), in slab geometries. We find that substantial slab thickness and Brillouin zone sampling is needed for convergence. Our results show that the surface layer contracts in agreement with experiment, and that the direction of relaxation of the near surface layers oscillates with depth. Both the magnitude of the surface layer contraction and the relaxed surface energies are in good agreement with available experiments and previous simulations. The electronic structure of the surface samples shows distinct surface bands near the Fermi level that are strongly affected by atomic relaxation. The surface phonon spectra show distinct features that correspond to the binding strength of the surface atoms. We also calculate the formation energies of surface defects including adatoms and vacancies. Relaxation around the defects usually involves mainly the first-neighbor atoms, except on the (111) surface where atoms in up to three layers under the defect move significantly.

DOI: 10.1103/PhysRevB.68.035422 PACS number(s): 68.47.De, 73.20.At, 68.35.Ja, 68.35.Dv

I. INTRODUCTION

The NRL tight-binding (TB) total energy method[1,2] makes it possible to study finite temperature and surface properties of materials. Using this method, which gives both energetic and electronic structure information, we have studied the low-index surfaces of Nb. The electronic and vibrational properties of the bulk material have been the subject of numerous experimental[3–5] and theoretical[1,2,6–12] investigations. In particular the electronic band structure and the phonon dispersion curves or the phonon density of states have been studied extensively. From zero-temperature calculations it appears that the measured mode at 2 THz is due to a Kohn anomaly and the maximum phonon frequency is below 7 THz,[3,13] while finite temperature calculations are rather limited. The electronic and structural properties of the Nb low-index surfaces have also been studied. Self-consistent pseudopotential calculations of the Nb(001) surface electronic density of states (EDOS) for the unrelaxed system[14,15] revealed strong surface features close to the Fermi level. A similar behavior was also found for Nb(110) by photoemission,[16–19] while to our knowledge there are no available data concerning the EDOS of the Nb(111) surface. Studies concerning the surface energies[1,2,9–12,20–23] and relaxation[22,24–27] found that the (110) surface has the lowest surface energy and that all three low index surfaces show a contraction of the surface layer. Some density functional theory (DFT) calculations using full-potential linear-muffin-tin orbitals (LMTO) and previous TB calculations underestimated the contraction of the Nb(001) surface layer as compared to photoelectron diffraction data.[22,25] Another DFT calculation using pseudopotentials, which correctly predicted the surface contraction, suggested that relaxation is important for accurately reproducing the experimental Nb(001) surface band structure.[24] Little or no data are available for the other surfaces. For the Nb(110) surface, although there are band structure angle-resolved photoemission data along one high-symmetry direction,[15,16,18,19] most of the experiments focus on the electronic properties of metals deposited on this face.[15,18] To our knowledge detailed studies concerning the electronic and vibrational properties of the Nb(110) and Nb(111) surfaces are rather scarce and there are no studies of the behavior of the surfaces in the presence of adatoms or surface vacancies. This is due to the fact that empirical interatomic potentials (e.g., the embedded atom method or second moment approximation) do not explicitly consider the electronic properties of the materials, while *ab initio* electronic structure calculations are impractical for a large number of atoms and k-points.

In this work we perform TB simulations to calculate structural, vibrational and electronic properties of the Nb body-centered-cubic (bcc) bulk and low-index surfaces in presence of adatoms or vacancies. We extend the original NRL-TB procedure[1] by incorporating quadratic polynomials into the functional form of the Slater-Koster (SK) matrix elements and limiting the short range behavior of the SK overlap matrix elements.[28] In addition, we augment the fitting database with information about the simple cubic (SC) structure and phonon frequencies at the *P* and *N* high symmetry points. We begin validating the TB Hamiltonian by calculating some zero-temperature bulk quantities such as elastic constants, phonon modes and vacancy formation energy as well as finite temperature properties including thermal expansion coefficient, phonon density of states and mean squared displacements. Taking advantage of the computational efficiency of the TB approach, we systematically test the convergence of our results with respect to system size and sampling of the Brillouin zone (BZ). We find that thick slabs and a high density of k-points are required to converge our results for structural, electronic and vibrational surface

TABLE I. Equilibrium lattice constant (a), bulk modulus (B), elastic constants (c_{ij}) and phonon frequencies for the Nb BCC bulk system, comparing the results of our TB parametrization (TB) with experimental data, previous TB results (TB_o), and first principles LAPW and PP calculations.

			Equation of state		
	Expt. (Refs. 29 and 30)	TB_o (Ref. 1)	LAPW (Ref. 1)	PP (Ref. 7 and 8)	TB
a (Å)	3.30	3.25	3.25	3.26	3.25
B (Mbar)	1.70	1.87	1.93	1.82	1.85
			Elastic constants (GPa)		
	Expt. (Ref. 5)	TB_o (Ref. 2)	LAPW (Ref. 2)		TB
c_{11}	246	204	230	-	277
c_{12}	139	137	122	-	139
c_{44}	29	55	25	-	37
			Bulk phonon frequencies (THz)		
k-point	Expt. (Ref. 3)	TB_o	LAPW (Refs. 6 and 11)	PP (Ref. 7 and 8)	TB
H	6.49	6.48 (Ref. 2)	6.48	6.4	6.28
P	5.04	6.53	5.97–6.07	-	5.73
N-T [001]	5.07	5.34	4.86	5.1	4.88
N-L [110]	5.66	7.64	5.02–5.36	-	5.92
N-T $[1\bar{1}0]$	3.93	3.88	4.08	4.3	4.41
Δ-L $\frac{1}{2}$[010]	5.73	6.36	-	-	5.92
Δ-T $\frac{1}{2}$[100]	3.55	4.28	-	-	3.59

properties. Finally, we show how the presence of adatoms or surface vacancies affects the morphology of the Nb surface atoms. In Sec. II we discuss the method, including its validation for many bulk properties. In Sec. III we present surface structural, electronic and vibrational properties as well as adatom and surface vacancies energetics and geometries. In Sec. IV we summarize our results.

II. METHOD

A. Tight binding method and fitting

The basic approach of the NRL-TB method is to represent the Slater-Koster Hamiltonian using simple functional forms with the parameters chosen to reproduce the electronic structure and total energy of first-principles calculations over a wide range of pressures and structures. Since the functional forms of the parameters used in the NRL scheme have already been presented,[1,2] we will not discuss them here. In that previous work, a set of Nb TB parameters (TB_o) (Ref. 46) was used,[1,2,11] and found to satisfactorily reproduce some Nb bulk properties. However, these parameters were found to overestimate the bulk phonon frequencies at the P and N high symmetry points. In this work we use a newer functional form for the overlap and hopping matrix parameters.[28] We augment the fitting database with linearized augmented plane wave (LAPW) results for the energy and band structure of the SC structure and the energy of frozen phonon calculations corresponding to the N and the P high symmetry points at a displacement of 0.005 lattice coordinates. In all cases we use a uniform regular k-point mesh that corresponds to 89, 55 and 84 k points in the irreducible part of the face-centered cubic (fcc) lattice, the bcc lattice and the SC BZ, respectively. In addition we used a set of 35 and 105 k points for energy and eigenvalues corresponding to the P and N symmetry points. The bcc total energy is weighted about 1000 times more than a single band or the frozen phonon energies. The average rms error of the six lowest bands is approximately 10 mRy and less than 0.5 mRy for the total energies.

B. Validation and bulk properties

A direct result of the fitting procedure is the accurate determination of the EDOS, the band structure, the equilibrium lattice parameter and the bulk modulus. In Table I, we show that the last two quantities are in agreement with available experimental[29,30] and theoretical data.[1,2,7,8,11] To validate the TB parameters we evaluate the elastic constants c_{11}, c_{12}, and c_{44}.[31] We calculate the phonon frequencies at the Γ, H, P, N and middle Δ points of the BZ using the frozen phonon method.[32] These results are summarized in Table I along with the corresponding quantities found independently by the LAPW method,[1] with the first-principles pseudopotential method,[8,7] and with the available experimental data.[3,5] As we can see in Table I, our predictions are in very good agreement with both the LAPW results and the experimental data for every quantity, including the elastic constants[5] and the phonon frequencies (at the Γ, H, middle Δ points and the N transverse frequencies) that were not included in the fitting database. In Table I we also present TB_o results,[1,2,11] where phonon modes were not included in the fitting procedure. We observe that the values obtained using the new TB parameters, which include the phonon frequencies at the P and the N symmetry points are in better agreement with the experimental and LAPW data.

Another test of the TB Hamiltonian that is farther from the fitting configurations, but which can be compared to first principles calculations and experiments, is the vacancy for-

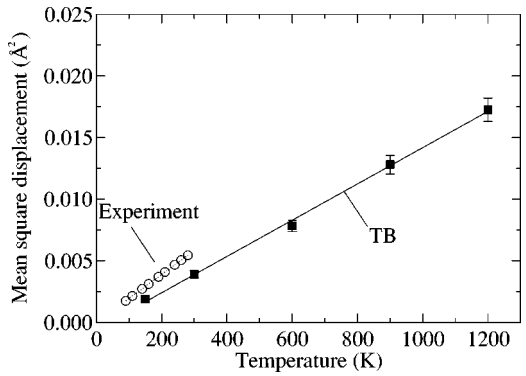

FIG. 1. Mean squared displacement of Nb atoms. Squares and circles stand for the TB and the experimental data respectively.

mation energy. Using the supercell total energy method[33] and unconstrained conjugate gradient energy minimization using TB forces we compare the ideal and relaxed vacancy formation energy. We find that a supercell with $125-1$ atoms and 32 k points is sufficient for a well converged calculation without any vacancy-vacancy interactions. The calculated values for the vacancy formation energy are 3.53 and 3.23 eV for unrelaxed and relaxed systems, respectively. Surprisingly, these results are not as close to the experimental values (2.65 ± 0.3 eV) as our previous TB_o calculations 2.84 and 2.82 eV.[1] We also calculated the formation energy of a divacancy by removing two neighboring atoms from a supercell of 125 atoms. We found 6.78 and 6.37 eV for the unrelaxed and the relaxed system, respectively. There are no experimental results to compare the divacancy calculations.

To test the finite temperature properties of the TB Hamiltonian we performed molecular dynamics (MD) simulations[34] of a 343-atom unit cell with eigenstates evaluated only at the Γ point. From these simulations we extracted the thermal expansion coefficient α (Ref. 35) and the atomic mean squared displacement,[36] which can be compared to experimental data. The calculated α of 5.310^{-6} K^{-1} is reasonably close to the experimental value 7.110^{-6} K^{-1}.[29,30] In Fig. 1, we present the mean square displacement of the Nb atoms along with experimental data derived from Debye-Waller factor measurement.[4] We observe that the calculated $\langle u^2 \rangle$ are consistent with the experiment, with the best agreement at low temperatures.

III. SURFACE PROPERTIES

A. System size effects in slab geometries

Using the validated TB Hamiltonian we study the structure of a surface by simulating slabs that are periodically replicated in only two dimensions. The configurations consist of a single primitive surface unit cell in-plane and a number of atomic layers normal to the surface with vacuum on both sides of the slab. We perform a set of relaxed TB calculations in order to determine the minimal number of layers and k-points for well converged calculations. In Fig. 2, we present the interatomic distances as a percentage of the bulk interlayer distance (BID) for three different slabs of the Nb(111) surface sampled with 120 ($20\times12\times1$) in-plane k points. We observe an oscillatory behavior for the interatomic distances that converges to the BID for a slab of 36 atomic layers. This suggests that in order to accurately describe the interlayer distance of the bulk atomic layers and the bulk structural properties of the slab, we need at least a 36-layer slab for the Nb(111) surface. The relaxation of the surface and subsurface layers oscillates as a function of depth. The magnitude of the relaxation depends on the thickness of the slab. Thinner slabs, for example with 12 or 18 layers [Figs. 2(a) and 2(b)], show a smaller surface layer contraction of -22% compared to -25% for the 36-layer slab. Similar behavior was also observed for the (001) and (110) surfaces.

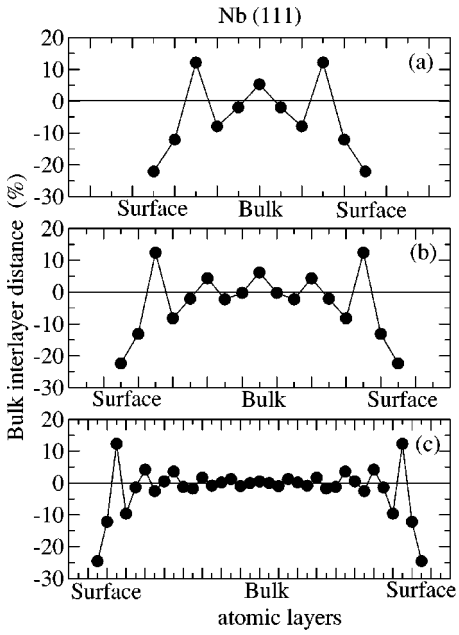

FIG. 2. Interatomic distance as a percentage of the bulk interlayer distance for (a) 12, (b) 18, and (c) 30 atomic layer slabs of Nb(111) surface.

In order to clearly present this behavior, in Fig. 3 we plot the (001) surface layer contraction (SLC) and the BID as a function of the number of layers for meshes of 50 ($10\times10\times1$), 113 ($15\times15\times1$) and 200 ($20\times20\times1$) k points in the irreducible part of the surface BZ. As the number of atomic layers increases convergence is achieved for the SLC. We note that we need at least 20 atomic layers and 113 k points for convergence of the SLC. In addition, it is worth noting that the absolute value of SLC for the six-layer slab, even using 200 k points (-9.3%), is smaller than the 20-layer slab (-11.65%) suggesting that a six-layer slab may not be able to accurately describe this important surface quantity. This dependence could explain the underestimates of SLC found by other TB quenched molecular dynamics (QMD) (Ref. 26) and DFT (Ref. 22) calculations in which six and seven layer slabs were used, respectively. In Table II, we present the Nb (001) SLC. The thin k-point converged slabs are in agreement with comparable DFT (Ref. 22) calculations (the SLC is -9.3%), but underestimate the experimental results. The converged Nb (001) surface layer contraction for the 20 layer slab (-11.65%) is consistent with photoelectron diffrac-

TABLE II. Surface layer contraction (SLC) of the low index Nb surfaces with respect to the bulk interlayer spacing (%).

Orient.	Expt. (Ref. 25)	TB-QMD (Ref. 26)	FP-LMTO (Ref. 22)	PP (Refs. 24 and 25)	TB
(001)	-13 ± 5	-6.3	-9.3	-12	-11.7
(110)	-	-3.6	-3.7	-	-5.8
(111)	-	-21.5	-9.4	-	-24.8

tion studies[25] despite the fact that no surface property was included in the fitting data of the TB parameters. The BID, Fig. 3(b), shows similar convergence behavior to the SLC. In Table II, we also present the surface layer contraction of the (110) surface (convergence was found for 140 ($14\times20\times1$) in-plane k-points and 20 atomic layers) and the (111) surface, along with the corresponding underestimated values of the TB-QMD and DFT calculations. It is worth noting that one of the reasons that previous studies used a seven layer slab is because a DFT calculation in a system with more than 20 atomic layers and many *k* points requires a lot of computational time. This is a clear advantage of the TB method, which can quickly handle a large number of atoms while providing both the total energy and detailed electronic structure.

B. Surface energy

The surface energy (γ) for both relaxed and unrelaxed systems is calculated by comparing the energy of the slab geometry to an equivalent bulk system. In our calculations we use the bulk TB equilibrium lattice parameter. In Tables III and IV we present the surface energy for the unrelaxed and relaxed systems, respectively, in good agreement with the available experimental[10,21] and theoretical data.[1,9–12,20,22,23] For the unrelaxed system the surface energy calculations using the new TB parameters are in better agreement with the full potential LAPW calculations[9] and the full charge density LMTO calculations[12] than the results using the TB_o parameters. In addition, the surface energies of the relaxed system are in better agreement with the experimental data[10,21] and the DFT calculations[22] than the corresponding values using empirical potentials.[20,23] Among the low index surfaces, we find that the Nb (110) surface is energetically favored and that it exhibits the smallest surface layer contraction. This result suggests that this surface orientation is most stable and suitable for deposition in epitaxial growth. Indeed, there are many studies using the Nb(110) surface for Pd,[19,37–39] Pt[18] and Cu deposition.[40] These results are also consistent with low energy electron microscopy on the Nb(011) vicinal surface,[41,42] which suggested that the observed formation of {110} nanofacets arises from the low surface energy of Nb(110) surface.

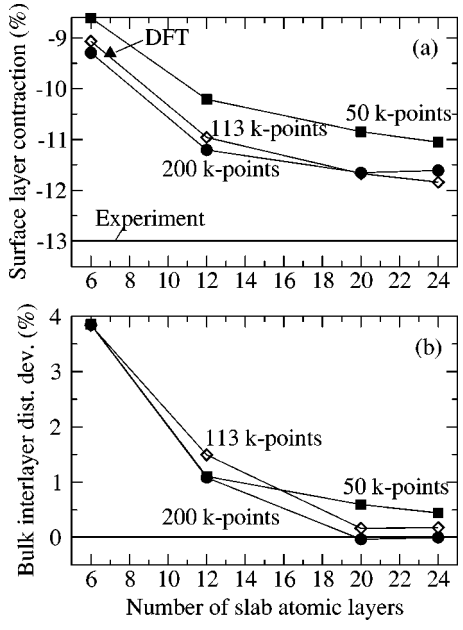

FIG. 3. System size effect on the Nb(001) surface: (a) Surface layer contraction and (b) bulk interlayer distance as a percentage of the perfect bulk interlayer distance as a function of slab thickness, for various *k*-point meshes (squares, diamonds, circles), compared with DFT (triangle) and experiment (solid line).

C. Surface electronic density of states

The surface EDOS of the Nb low-index surfaces is calculated using an energy histogram weighting each electronic eigenvalue by the projection of the corresponding eigenvectors on the surface atoms. In Fig. 4, we present this quantity for the (001), (110) and (111) Nb surfaces for both the relaxed and unrelaxed slabs along with the bulk EDOS. The slab calculation EDOS includes contributions from both surface resonances, which are bulk-like, and from surface states, which typically form narrow bands and lead to the sharp peaks seen in the figure. We find surface character below the Fermi level (-0.2–0.0 Ry) for the Nb(001) surface, Fig. 4(b), in agreement with angle-resolved photoelectron spectroscopy,[24,43] while strong surface features are also found above the Fermi level (up to 0.2 Ry), in agreement with a DFT calculation.[14,15] The (110) surface EDOS exhibits peaks around -0.035 and -0.12 Ry below the Fermi level, in agreement with other TB calculations (-0.037 and -0.12

TABLE III. Surface energy γ of the unrelaxed Nb low index surfaces (J/m^2).

Orient.	TB_o (Ref. 1)	FLAPW (Ref. 9)	FCD-LMTO (Ref. 12)	TB
(001)	2.37	3.1	2.858	2.887
(110)	2.10	2.9	2.685	2.693
(111)	2.44	-	3.045	3.067

TABLE IV. Surface energy γ of the relaxed Nb low index surfaces, and experimental polycrystalline average γ (J/m^2).

Orient.	Expt. (Refs. 10 and 21)	DFT (Ref. 22)	EP (Ref. 20)	EAM (Ref. 23)	MEAM (Ref. 10)	TB
poly	2.3–2.7					
(001)	-	2.86	1.96	1.97	2.02	2.765
(110)	-	2.36	1.67	1.81	1.87	2.666
(111)	-	-	-	-	2.02	2.798

Ry) for the unrelaxed system[37,39] and photoemission data (-0.029 and -0.18 Ry).[18] Above the Fermi level, we observe surface character from +0.1 up to +0.25 Ry whereas photoemission data reveal two main peaks at +0.09 and +0.26 Ry.[19] For the (111) surface EDOS, we found strong surface character around -0.03 and +0.15 Ry in agreement with DFT calculations.[22]

In summary, we find that for the three low-index surfaces, the EDOS exhibits strong surface character close to the Fermi level compared to the Nb bulk EDOS. In addition, we observed a small shift to higher energies for the relaxed surface compared to the unrelaxed. For all surfaces and the bulk, the states below 0.6 Ry have mainly *d* character, while the higher energy states have mainly *p* character.

D. Surface band structure

For a more detailed picture of the surface electronic structure we calculate the surface band structure along the crystallographic directions of the surface first BZ.[44] We define states with significant surface character as those states where at least 10% of the wavefunction amplitude squared is on the surface atoms and less than 1% is on each bulk layer. This definition does not allow us to distinguish between true surface states, which are different in energy or symmetry than bulk states, and surface resonances, which are simply bulk states with enhanced intensity at the surface. To compare the experimental data to our calculations we present in Fig. 5(a)

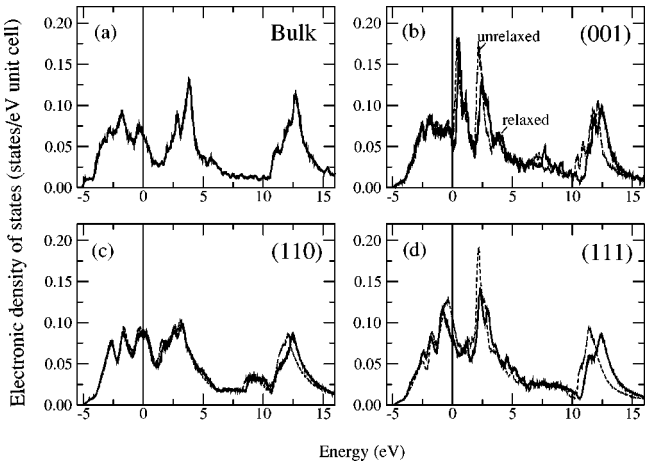

FIG. 4. Electronic density of states: (a) bulk, (b) (001) surface, (c) (110) surface, and (d) (111) surface. The dashed lines indicate unrelaxed geometries, and the solid lines indicate relaxed geometries.

the Nb(001) surface band structure along the $\bar{X}\rightarrow\bar{M}$ direction and below the Fermi level. We observe that the presence of the surface stimulates some new states mainly situated in the areas that are free of bulk modes (i.e. true surface states), in agreement with the corresponding surface EDOS [Fig. 4(b)], theoretical results[14,15] and angle-resolved photoelectron spectroscopy data.[24,25] Relaxation shifts these surface states closer to the experimental data. Moreover, some of the

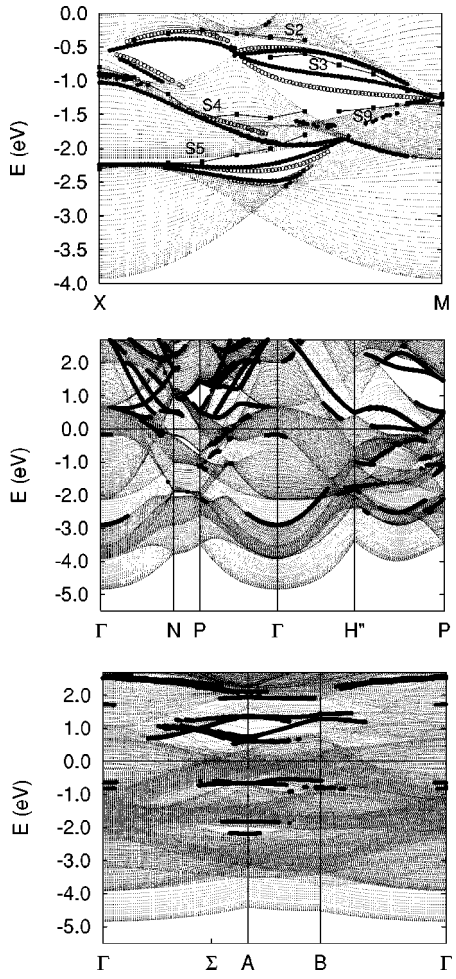

FIG. 5. Electronic band structure along high symmetry directions. Filled and open circles indicate surface states (as defined in the text) of the relaxed and the unrelaxed configuration, respectively. Squares correspond to the experimental data. Panel (a) shows results for the (001) surface, (b) for the (110) surface, and (c) for the (111) surface. The energies of the eigenstates have been uniformly shifted to set the Fermi level to zero.

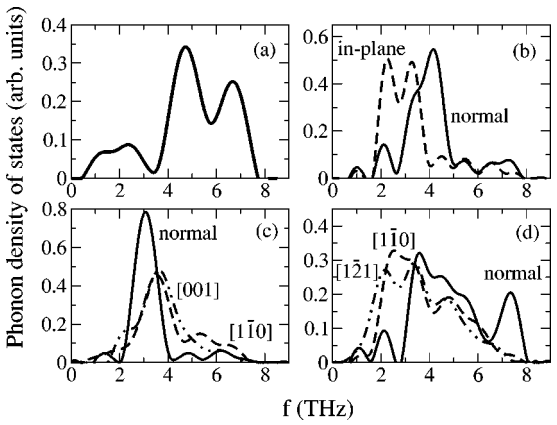

FIG. 6. Phonon density of states at 300 K: (a) bulk, (b) (001) surface, (c) (110) surface, and (d) (111) surface. For surfaces (b)–(d) the solid lines are the PDOS for vibrations normal to the surface, and dashed and dash-dotted lines are the PDOS for in-plane vibrations.

experimental surface states (e.g. the S9) are missing in the unrelaxed system. These results agree with previous work in which a comparison between the same experimental data and self-consistent calculations showed better agreement with the experimental surface for the relaxed configuration.[25,24] Finally, it is worth emphasizing that although we did not include any LAPW results for surfaces in the fitting database we satisfactorily reproduce the surface band structure of the Nb(001) surface.

In Fig. 5(b), we present the (110) surface band structure for the relaxed system along the $\bar{\Gamma}\rightarrow\bar{N}$, $\bar{N}\rightarrow\bar{P}$, $\bar{P}\rightarrow\bar{\Gamma}$, $\bar{\Gamma}\rightarrow\bar{H}'$, and $\bar{H}'\rightarrow\bar{P}$ directions. The point $\bar{H}'$ is situated at $\frac{3}{4}$ of the $\bar{\Gamma}\bar{H}$ vector. We can identify a surface state or resonance that is related to the $\bar{\Gamma}$ point situated around -0.2 Ry below the Fermi level having mainly *s* and *d* character. In addition, we observe some states around -0.035 Ry in agreement with the surface EDOS [Fig. 4(c)], other TB calculations and experimental data,[16–19] as well as states around -0.12 Ry that are mainly situated close to the $\bar{P}$ point. In Fig. 5(c), we present the (111) surface band structure for the relaxed system. The $\bar{\Gamma}\rightarrow\bar{A}$ and $\bar{B}\rightarrow\bar{\Gamma}$ directions are parallel to the $[\bar{1}01]$ and $[\bar{1}\bar{1}2]$ directions.[44] The $\bar{A}$ point is situated at the $\frac{2}{3}$ of the $\bar{\Gamma}\bar{N}$ vector while the $\bar{B}\bar{\Gamma}$ vector's length is equal to $\frac{1}{2}\sqrt{\frac{2}{3}}$ of the lattice constant. We observe some surface states or resonances that cross at the $\bar{A}$ point at -0.15 and -0.03 Ry, and around +0.1 Ry, in agreement with our (111) surface EDOS results. To our knowledge there are no experimental or theoretical data available for comparison.

E. Surface phonons at 300 K

The total phonon density of states (PDOS) can be easily calculated using the TB MD trajectories[45] by Fourier transforming the corresponding velocity-autocorrelation function. In Fig. 6(a) we present the PDOS of the bulk system calculated from a MD simulation of a 448- atom supercell sampled with six *k* points in the full BZ. Starting from a well equilibrated configuration, three trajectories of 500-2-fs time steps each were used to gather data. The bulk PDOS is consistent with the eighth-neighbor model based on the Born–von Karman theory using experimental data[3] at room temperature. It is worth noting that we also observe the phonon mode at 2 THz which was attributed to a Kohn anomaly.[13] The surface PDOS is calculated from MD simulations of slabs with 25 atoms per layer, 20 layers, and four *k* points in the surface BZ for the (100) surface, 32 atoms per layer, 14 layers, and six *k* points for the (110) surface, and 18 atoms per layer, 30 layers, and six *k* points for the (111) surface. As for the bulk system described above, data was gathered from three different 500 time-step trajectories. The symmetry of the (001) surface is reflected in its PDOS in the in-plane directions, Fig. 6(b), while the geometrical anisotropy is visible in the PDOS of the (110) and (111) surfaces, Figs. 6(c) and 6(d), respectively. The high frequency bulk mode (around 6.7 THz) is absent in the PDOS of the (001) and (110) surfaces indicating that these surface atoms are less tightly bound than the bulk atoms. In all cases the main in-plane surface modes are situated around 3–4 THz where there are no bulk phonon modes. The (111) surface has different PDOS morphology, Fig. 6(d), than the other two surfaces, including a new surface mode around 7.3 THz polarized normal to the surface direction. This mode has a higher frequency than any bulk mode indicating that the (111) surface atoms are more tightly bound in the surface normal direction than the bulk atoms.

F. Surface defects

Surface defects govern the evolution of surfaces at finite temperatures. Such defects can be simulated by creating slab configurations with several surface unit cells and placing one adatom or vacancy on the surface. The computational efficiency of the TB method makes it possible to use very large supercells, minimizing the effects of defect-defect interactions. We find that supercells mentioned in the previous section, containing 20, 14, and 30 atomic layers with 25, 32, and 18 atoms per layer for the (001), (110), and (111) surfaces, respectively, are sufficient to eliminate the interaction between the periodic images. We calculate binding energies for the Nb adatoms of 6.63, 5.79, and 7.23 eV on the (001), (110), and (111) surfaces, respectively. The corresponding measured value of the cohesive energy for the bulk system is 7.47 eV.[29,30] The Nb adatom occupies the fourfold position on the (001) and (110) surface, while on the (111) surface it occupies a fcc position rather than a hcp position. The presence of the adatom affects the relaxed positions of the neighboring atoms. In Fig. 7, we show a schematic atomic representation of the three low index surfaces with a Nb adatom. We observe that the adatom mainly affects the relaxed positions of the first neighboring atoms and that this influence depends on the surface geometry. The first neighboring surface atoms move toward the adatom on the (001) and (111) surfaces. On the (110) surface substrate atoms along the $[1\bar{1}0]$ direction move toward the adatom while the substrate atoms along the [001] move away from the adatom. The second layer atom that is situated below the adatom normal

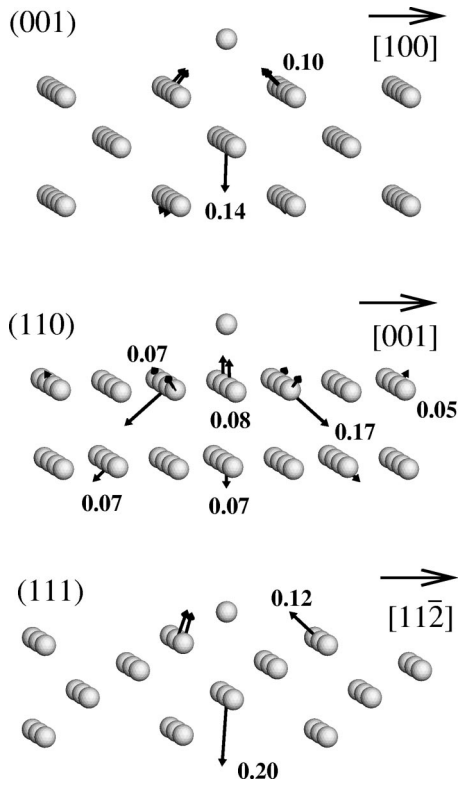

FIG. 7. Visualization of the (001), (110), and (111) Nb surfaces with an adatom. The arrows on the atoms represent the direction of the relaxation due to the presence of the adatom. Numbers on the atoms correspond to the deviation of the atomic distances in Å from the relaxed flat surface. Large arrows correspond to the in-plane directions [100], [001], and [11$\bar{2}$] direction for the three surfaces, respectively.

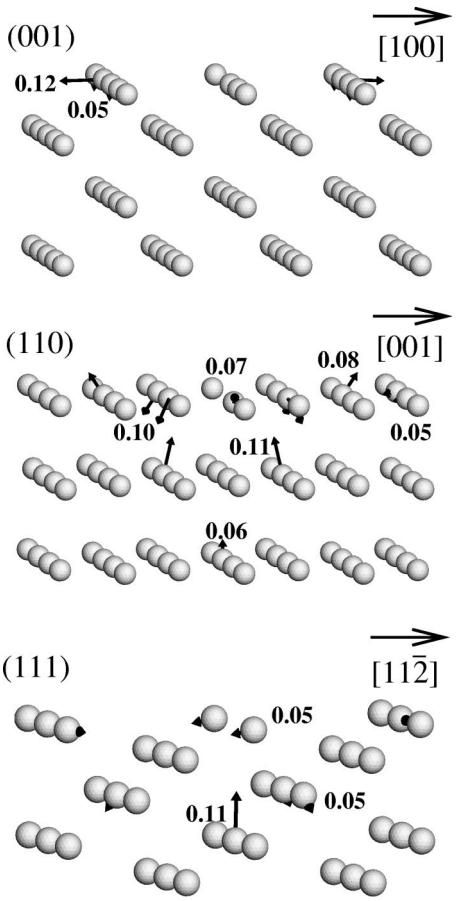

FIG. 8. Visualization of the (001), (110), and (111) Nb surfaces with a vacancy. The arrows on the atoms represent the direction of the relaxation due to the presence of the vacancy. Numbers on the atoms correspond to the deviation of the atomic distances in Å from the relaxed flat surface. Large arrows correspond to the in-plane directions [100], [001], and [11$\bar{2}$] direction for the three surfaces respectively.

to the (001) surface direction moves strongly away from the Nb adatom. This relaxation is also present, although smaller in magnitude, on the (110) and (111) surfaces. The adatom on the (111) surface causes the third layer atom (situated below the adatom) to relax away, while on the (110) and (111) surface its influence is negligible at the third layer. The presence of the adatom does not affect the positions of the fourth layer atoms for the low index surfaces.

We calculate the formation energies of Nb surface vacancies in the (001), (110), and (111) surface layers of 0.99, 1.13, and 0.18 eV, respectively. These values are significantly below the bulk vacancy formation energy of 3.24 eV (Sec. I). As for the adatoms, the presence of a surface vacancy affects the relaxed positions of the neighboring surface atoms. In Fig. 8, we show the schematic atomic representation of the three low index surface in presence of a surface vacancy. In most cases only the first neighbors of the vacancy relax significantly. On the (001) surface the neighbors in the surface layer relax away from the vacancy. On the (110) surface the relaxation extends deeper into the slab. First-layer atoms relax away from the vacancy, while second- and third-layer atoms relax toward it. On the (111) surface first-layer atoms relax in plane, pairing to reduce the local symmetry to threefold. Third-layer atoms move slightly away from the vacancy, while the fourth-layer atom, directly beneath the vacancy, moves toward it. As these results show, the presence of surface defects causes significant relaxation in the substrate, in some cases extending to second neighbors or four layers into the substrate. This relaxation generates strain fields in the solid that lead to interactions between surface defects. These interactions could significantly influence the energetics and kinetics of atoms during deposition, and therefore influence the morphology of the growing surface.

IV. SUMMARY

We have used the NRL-TB method to study the properties of Nb low index surfaces. The TB parameters we use are determined from a fit to first principles LAPW calculations of bulk structure energy and phonon frequencies at the *P* and *N* symmetry points. We determine that these parameters satisfactorily reproduce zero temperature bulk properties such as electronic density of states, elastic constants, phonon frequencies and vacancy formation energy as well as the thermal expansion coefficient, the phonon density of states at 300 K and atomic mean squared displacements. Using these

parameters we studied the geometry of the surface layers, and find that many layers and *k* points are needed for converged results. The converged surface energies and surface-layer contractions are in very good agreement with the available experimental data. The ability of the TB method to handle a large number of atoms while providing detailed electronic structure information makes these well-converged simulations practical. The surface electronic density of states and the surface band structure show distinct features close to the Fermi level that are strongly affected by relaxation, in agreement with available experimental and other theoretical studies. The surface phonon densities of states of the three low index surfaces show different structures, which we relate to the surface geometry and bonding. Finally, we observe that the presence of adatoms or vacancies on the low index surfaces mainly affects the positions of the neighboring atoms several layers into the substrate. The relaxation of the substrate atoms will lead to interactions between surface defects and influence surface morphology during deposition.

[1] M.J. Mehl and D.A. Papaconstantopoulos, Phys. Rev. B **54**, 4519 (1996).

[2] R.E. Cohen, M.J. Mehl, and D.A. Papaconstantopoulos, Phys. Rev. B **50**, 14 694 (1994).

[3] Y. Nakagawa and A.D.B. Woods, Phys. Rev. Lett. **11**, 271 (1963).

[4] L.M. Peng, G. Ren, S.L. Dudarev, and M.J. Whelan, Acta Chem. Scand. **52**, 456 (1996).

[5] G. Simmons and H. Wang, *Single Crystal Elastic Constants and Calculated Aggregate Properties: A Handbook* (MIT Press, Cambridge, 1971).

[6] J.R. Anderson, D.A. Papaconstantopoulos, J.W. McCaffrey, and J.E. Schirber, Phys. Rev. B **7**, 5115 (1973).

[7] K.-M. Ho, C.L. Fu, and B.N. Harmon, Phys. Rev. B **29**, 1575 (1984).

[8] Y. Chen, C.-L. Fu, K.-M. Ho, and B.N. Harmon, Phys. Rev. B **31**, 6775 (1985).

[9] M. Weinert, R.E. Watson, J.W. Davenport, and G.W. Fernando, Phys. Rev. B **39**, 12 585 (1989).

[10] M.I. Baskes, Phys. Rev. B **46**, 2727 (1992).

[11] D. A. Papaconstantopoulos and M. J. Mehl, in *Stability of Materials*, Vol. 355 of *NATO Advanced Study Institute, Series V. Physics*, edited by A. Gonis, P. E. A. Turchi, and J. Kudrnovsky (Plenum, New York, 1996), p. 325.

[12] L. Vitos, A.V. Ruban, H.L. Skriver, and J. Kollar, Surf. Sci. **411**, 186 (1998).

[13] J. Peretti, I. Pelah, and W. Kley, Phys. Lett. **3**, 105 (1962).

[14] S.G. Louie, K.-M. Ho, J.R. Chelikowsky, and M.L. Cohen, Phys. Rev. Lett. **37**, 1289 (1976).

[15] S.G. Louie, K.-M. Ho, J.R. Chelikowsky, and M.L. Cohen, Phys. Rev. B **15**, 5627 (1977).

[16] R.J. Smith, Phys. Rev. Lett. **45**, 1277 (1980).

[17] R.J. Smith, Solid State Commun. **37**, 725 (1981).

[18] X.-H. Pan, M.W. Ruckman, and M. Strongin, Phys. Rev. B **35**, 3734 (1987).

[19] X. Pan, P.D. Johnson, M. Weinert, R.E. Watson, J.W. Davenport, G.W. Fernando, and S.L. Hulbert, Phys. Rev. B **38**, 7850 (1988).

[20] G.J. Ackland and M.W. Finnis, Philos. Mag. A **54**, 301 (1986).

[21] F. R. de Boer, R. Boom, W. C. M. Mattens, A. R. Miedema, and A. K. Niessen, *Cohesion in Metals: Transition Metal Alloys* (North-Holland, Amsterdam, 1988).

[22] M. Methfessel, D. Hennig, and M. Scheffler, Phys. Rev. B **46**, 4816 (1992).

[23] A.M. Guellil and J.B. Adams, J. Mater. Res. **7**, 639 (1992).

[24] B.-S. Fang, W.-S. Lo, T.-S. Chien, T.C. Leung, C.Y. Lue, C.T. Chan, and K.M. Ho, Phys. Rev. B **50**, 11 093 (1994).

[25] W.-S. Lo, T.-S. Chien, B.-S. Fang, C.M. Wei, and W.N. Mei, Surf. Rev. Lett. **5**, 1035 (1998).

[26] J.S. Luo and B. Legrand, Phys. Rev. B **38**, 1728 (1988).

[27] C. E. Lekka, G. A. Evangelakis, N. I. Papanicolaou, and D. A. Papaconstantopoulos, in *Atomistic Aspects of Epitaxial Growth* Vol. 65 of *NATO Science Series: II: Mathematics, Physics and Chemistry* (Kluwer Dordrechts, 2002), pp. 43–49.

[28] D. A. Papaconstantopoulos, M. J. Mehl, S. C. Erwin, and M. R. Pederson, in *Tight-Binding Approach to Computational Materials Science*, edited by P. E. A. Turchi, A. Gonis, and L. Colombo, MRS Symposia Proceedings, No. 491 (Materials Research Society, Warrendale, PA, 1998) pp. 221–230.

[29] C. Kittel, *Introduction to Solid State Physics* (Willey, New York, 1989).

[30] N. W. Ashcroft and N. D. Mermin, *Solid State Physics* (Saunders College, Philadelphia, 1976).

[31] M. J. Mehl, B. M. Klein, and D. A. Papaconstantopoulos, in *Intermetallic Compounds*, edited by J. H. Westbrook and R. L. Fleischer (Wiley, New York, 1994), Vol. 1.

[32] B.M. Klein and R.E. Cohen, Phys. Rev. B **45**, 12 405 (1992).

[33] M.J. Mehl and B.M. Klein, Physica B **172**, 211 (1991).

[34] F. Kirchhoff, M.J. Mehl, N.I. Papanicolaou, D.A. Papaconstantopoulos, and F.S. Khan, Phys. Rev. B **63**, 195101 (2001).

[35] N. Bernstein, M.J. Mehl, D.A. Papaconstantopoulos, N.I. Papanicolaou, M.Z. Bazant, and E. Kaxiras, Phys. Rev. B **62**, 4477 (2000).

[36] J. Huang, M. Meyer, and V. Pontikis, Phys. Rev. B **42**, 5495 (1990).

[37] V. Kumar and K.H. Bennemann, Phys. Rev. B **26**, 7004 (1982).

[38] V. Kumar and K.H. Bennemann, Phys. Rev. B **28**, 3138 (1983).

[39] M. El-Batanouny, D.R. Hamann, S.R. Chubb, and J.W. Davenport, Phys. Rev. B **27**, 2575 (1983).

[40] M. El-Batanouny and M. Strongin, Phys. Rev. B **31**, 4798 (1985).

[41] C.P. Flynn and W. Swiech, Phys. Rev. Lett. **83**, 3482 (1999).

[42] C.P. Flynn, W. Swiech, R.S. Appleton, and M. Ondrejcek, Phys. Rev. B **62**, 2096 (2000).

[43] B.-S. Fang, C.A. Ballentine, and J.L. Erskine, Phys. Rev. B **38**, 4299 (1988).

[44] M.-C. Desjonqueres and D. Spanjaard, *Concepts in Surface Physics* (Springer, Berlin, 1998).

[45] N.I. Papanicolaou, I.E. Lagaris, and G.A. Evangelakis, Surf. Sci. **337**, L819 (1995).

[46] The NRL-TB parameters for Nb are available at http://cst-www.nrl. navy. mil/bind/nb. html.